Chemical Engineering Journal 474 (2023) 145635

Contents lists available at ScienceDirect

Chemical Engineering Journal

journal homepage: www.elsevier.com/locate/cej

Unique hierarchical structures of one dimensional lepidocrocite titanate with cation-exchangeable sites for extraordinary selective actinide capture for water purification

Lin Wang [a,1], Hussein O. Badr [b,1], Yang Yang [a,c,1], Jacob H. Cope [b], Enzhao Ma [a], Jiafeng Ouyang [a], Liyong Yuan [a], Zijie Li [a], Zhirong Liu [c], Michel W. Barsoum [b,*], Weiqun Shi [a,*]

[a] Laboratory of Nuclear Energy Chemistry, Institute of High Energy Physics, Chinese Academy of Sciences, Beijing 100049, China
[b] Department of Material Science and Engineering, Drexel University, Philadelphia, PA, USA
[c] School of Nuclear Science and Engineering, East China University of Technology, Nanchang 330013, China

ARTICLE INFO

Keywords:
Lepidocrocite titanate
One-dimensional nanofilaments
Bottom-up synthesis
Ion exchange
Actinide adsorption
Water purification

ABSTRACT

Removing actinide from wastewater to render it potable is an active and important area of research. Herein, using TiB_2 as an inexpensive and green precursor, we synthesized 100 g-scale hierarchical structures composed of ion-exchangeable one-dimensional lepidocrocite (1DL) titanate nanofilaments for efficient actinide capture. These new and unique titanate hierarchical structures (THSs) are stable at pH $\geq$ 2.0 and have a considerable U (VI) adsorption capacity of 424 mg/g at pH 4.0. The THSs also exhibit outstanding selectivity and high removal efficiency for U(VI) when excess competing ions (such as Ca^{2+}, Mg^{2+}, transition metal and lanthanide ions) coexist. The applicability assessment further demonstrates their superb purification ability (>25 ton/kg adsorbent) for U-contaminated drinking water. The uranium concentration can be reduced from 2500 ppb to 1 ppb in 60 s, which meets the drinking water interim standard recommended by World Health Organization. Besides, the used adsorbents can be regenerated by binary acid and salts mixtures for at least five cycles. Spectroscopic analysis confirmed that TMA^+ and Li^+ in the THSs are replaced by U(VI) through ion exchange at the initial stage of adsorption. The underlying microscopic removal mechanism was predominantly bidentate inner-sphere complexation, accompanied by a small amount of reductive immobilization. The overall results in this work provide new insight into the large-scale, low-cost and highly efficient applications of these 1DL THSs in environmental remediation and water purification.

1. Introduction

Nanostructured materials usually exhibit quite distinct physical and chemical properties when compared to their bulk counterparts owing to their small size and concomitant high specific surface areas (SSAs), unique morphologies and customizable terminations. Their applications, in turn, is widespread in energy, catalysis, environmental and sensing fields. In the aspect of environmental remediation, nano-adsorbents with different structures are promising candidates for efficient removal of various environmental pollutants in recent years due to their high SSAs, controllable defects, numerous active adsorption sites and connected pore structures [1–3].

One-dimensional (1D) carbon nanotubes [4,5], two-dimensional (2D) graphene [6,7] and transition metal carbides, MXenes [8–12], as well as porous metal organic framework materials [13], etc., have been widely explored for the removal of heavy metal ions, radionuclides, dye molecules and organic pollutants from water in relatively short times. These results have strongly promoted the rapid development of water purification/treatment related research using these nanomaterials. However, the latter have yet to find traction as nano-adsorbents compared with mature processes such as industrial membrane separation technology. The reasons are several and include selectivity, and the high cost of large-scale production. Therefore, there is an urgent need to develop new and advanced adsorption materials for water purification.

Titanium dioxide or titania (TiO_2) has often served as a stable model substrate for experimental sorption studies of environmental

* Corresponding authors.
E-mail addresses: barsoumw@drexel.edu (M.W. Barsoum), shiwq@ihep.ac.cn (W. Shi).
[1] L. Wang, H.O. Badr and Y. Yang contributed equally to this work.

https://doi.org/10.1016/j.cej.2023.145635
Received 2 June 2023; Received in revised form 17 August 2023; Accepted 23 August 2023
Available online 26 August 2023

contaminants such as radionuclides and humic acid [14–16], but its adsorption performance is limited by the low number of surface active sites. Other studies have shown that the adsorption performance of various TiO_2 adsorbents is related to their crystallographic phase, morphology, grain size, SSA, surface charges and surface impurities [16]. For instance, the experimental uranium (U) uptake capacity of crystalline TiO_2/ZrO_2 porous beads and defective TiO_{2-x} are only 40.2 mg/g and 65.4 mg/g, respectively [14,15]. It is worth noting that another type of titania-based materials featuring ion-intercalation, namely titanates, have also been evaluated as promising adsorbents for the enrichment and separation of radionuclides such as Sr, Cs, U and Th due to their higher ion-exchange capacity [17–22]. However, the literature indicates that the adsorption of U(VI) on multilayer, (ML), titanate nanotubes is significantly suppressed in the presence of competing ions such as Ca(II) [23], suggesting that the selectivity of titanate adsorbents still needs to be improved. At present, the related studies mainly focus on the functionalization and hybridization of titanate materials to improve their selectivity and uptake capacity [24,25]. Another potential problem with titanates is how to scale up, inexpensively, their green synthesis.

In search of a scalable protocol to prepare nanomaterials we developed a bottom-up synthesis approach that enables the low-cost, large-scale – in the kilogram range – production of metal oxide low-dimensional nanostructures [26,27]. For example, aqueous solutions of tetramethylammonium hydroxide (TMAH) – a common organic base with a variety of roles as reaction agent, intercalating agent, as well as a templating agent – was reacted with 6 different binary and ternary manganese (Mn) oxides and borides. The reaction transformed them into crystalline 2D birnessite flakes that are 2–3 atomic layers-thick and up to 500 nm across [27]. The electrochemical performances of these flakes in electrocatalysis and supercapacitor applications were found to be in line with other reports in the literature. In contrast to the latter – mostly prepared through top-down techniques – ours is significantly cheaper, simpler and starts with non-toxic, earth-abundant precursors [27,28].

Following the same synthesis method, but starting with water-insoluble Ti-containing compounds such as TiC, TiN, TiB_2 and $TiSi_2$, we produced 1D lepidocrocite titanate nanofilaments (NFs), henceforth referred to as 1DL NFs [26,29]. These 1DL NFs grow along the [1 0 0] direction and are truly one-dimensional in that their minimal cross sections are of the order of 5×7 Å^2 [29,30]. These extreme dimensions, in turn, appear to result in quantum confinement that blue-shifts the band gap energy, E_g, to 4 eV from $\approx$ 3.2 eV for rutile/anatase [26,31]. To date, the 1DL NFs have shown promise in energy storage applications such as lithium-ion and lithium-sulfur batteries [32], photocatalytic hydrogen production [69], biomedical cancer therapy [26], as well as in polymer nanocomposites [70].

Since TiB_2 powders can be fully converted to 1DL NFs in 3 to 5 days (d), we converted 100 g of commercial TiB_2 powders into 1DL NFs by reacting them with a TMAH aqueous solution at 80 °C for 5 d in a temperature-controlled shaker [30]. The as-synthesized entities are 5 – 30 μm across titanate hierarchical structures, THSs, with a sponge-like morphology – but at a much finer scale (see Fig. S1). In all cases, and regardless of the final morphology, the building unit, remains 1DL NFs [30,33]. In our first report, after neutralizing the product with ethanol, (EtOH), to pH $\approx$ 7, it was washed with a LiCl solution to exchange the TMA cations with Li^+. This was carried out to rid the system from TMA^+ cations and reduce the C-concentration. More recently we showed that if we simply allow the EtOH to evaporate after neutralizing the reaction products with EtOH, THSs were obtained [30]. To probe the importance of the exchangeable cations on the effectiveness of U adsorption, we started with ones of that had either TMA^+ (as processed) or Li^+ (LiCl washing) ions in the interfilamentous gallery space. These will henceforth be referred to as THS-T or THS-L, respectively.

This work's impetuous was our realization that our 1DL NFs are readily cation exchangeable where the TMA^+ cations – present in the interfilamentous gallery space after reaction – can be readily replaced with various mono- and divalent cations including H^+/H_3O^+, Li^+, Na^+, Mg^{2+}, Mn^{2+}, Fe^{2+}, Co^{2+}, Ni^{2+}, and Zn^{2+} ions [30]. This fact together with theoretical SSAs in the 1000 m^2/g range suggested that these 1DL NFs could also be quite effective in adsorbing dangerous actinide cations.

Here, U is selected as a representative actinide for removal mainly because of its important role in the nuclear fuel cycle and the long-term environmental hazards of this radiotoxic, chemically toxic and highly mobile element [34,35]. With the increase of nuclear industrial activities such as uranium ore mining, discarded tailing and uncontrolled discharge of nuclear waste [36,37], a large amount of U-containing wastewater is produced, which urgently needs to be treated to avoid large-area environmental pollution. In this work, the physicochemical properties of the 1DL THSs and their dispersion stability in water were carefully evaluated, and the U(VI) adsorption behavior of the materials and their practical application of water purification were systematically investigated. We find that our THSs have considerable U(VI) adsorption capacity, excellent selectivity, and ultrafast purification ability for low and medium concentrations of U-contaminated radioactive wastewater. In addition, the underlying microscopic adsorption mechanism between U(VI) and 1DL titanate was explored by advanced spectral techniques. This work demonstrates the first case of this 1DL ion-exchangeable THSs for the environmental remediation applications of typical radioactive contamination.

2. Results and discussions

2.1. Characterization of 1DL-based titanate hierarchical structures (THSs)

The experimental details can be found in the materials and methods section (see Supplementary Material). In brief, the 1DL-based THSs were prepared by shaking TiB_2 precursor powders in 25% TMAH aqueous solution at 80 °C for 5 d. THS-T and THS-L powders were, respectively, obtained either by only EtOH washing, or by EtOH washing followed by a LiCl treatment. Typical X-ray diffraction (XRD) pattern of THS-T (red line in Fig. 1a) is characterized by a set of 0*k*0 reflections along the stacking or *b*-axis with a *b* lattice parameter (*b*-LP) of 11.5 Å (calculated based on 020 peak centered at 2θ angle value of 7.7°), which is in good agreement with that of 2-Ti-atom-thick 1DL NFs assembly in our previous work [26,29]. It is important to note that in our previous work we indexed the low angle peaks as 00*l* peaks; more recent work suggests that they are 0*k*0 peaks instead and that the NFs configuration is -ABAB- which renders the peak located at 7.7° a 020 reflection[29,30]. In this case, the 1DL NFs are characterized by four peaks – (1 1 0), (1 3 0), (2 0 0), and (0 0 2) denoted in red in Fig. 1a. The latter two are *not* functions of the nature of the cations surrounding the NFs. These peaks are crystallographic in origin and can be used to calculate both the c- and a-lattice parameters of our 1DL NFs. The (1 3 0) and (1 1 0) peaks are a weak function of the nature of the cation between the NFs. In addition to these peaks, small peaks of unreacted TiB_2 (denoted by asterisks in Fig. 1a) were observed. After washing in a LiCl solution, the *b*-LP of THS-T at ~ 11.5 Å decreased to ~ 9.3 Å as a result of the Li^+ cations replacing their TMA^+ counterparts (Fig. 1a). Similar to other reports in the literature, Li ions intercalation favors an -AAA- type stacking, that slightly shifts the 110 peak position and vanishes the 130 peak [71,72]. X-ray photoelectron spectra (XPS) spectra in the N 1 s and C 1 s regions (Fig. 1h and 1i) and EDX analysis (Fig. S2) clearly show that the TMA^+ cations concentrations are significantly reduced after washing with LiCl solution. This was further confirmed when calcining the THS-L powders, at 800 °C, resulted in a mixture of $Li_{1.33}Ti_{1.67}O_4$ phase and rutile (Fig. S3). Calcining the THS-T, on the other hand, resulted in anatase and rutile (Fig. S3).

Typical scanning electron microscope (SEM) images of THS-T and THS-L powders shown in Fig. 1b-c and 1e-f, respectively, depict that

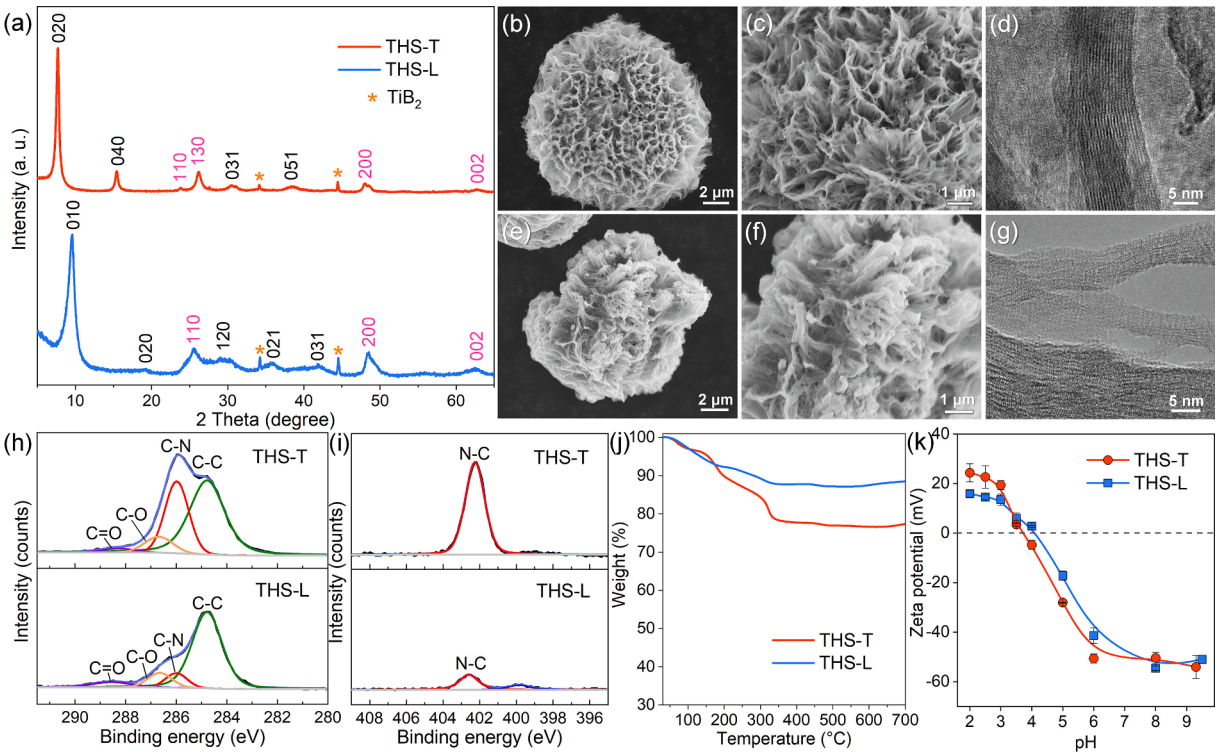

Fig. 1. Characterization of 1DL-based THSs. (a) Powder XRD patterns of THS-T and THS-L. (b-d) SEM and TEM images of THS-T. (e-g) SEM and TEM images of THS-L. (h, i) XPS spectra of THS-L and THS-T powders in (h) C 1s, and (i) N1s regions. TMA^+ cations show characteristic C − N and N − C bonds, and the C − C, C − O, and C = O peaks in (h) are attributed to adventitious carbon contamination. (j) Thermogravimetric results of THS-T and THS-L. (k) Zeta potentials vs. solution pH of THS-T and THS-L powders.

both have flower- or sponge-like morphologies with some particles being > 10 μm in lateral dimensions. The former has a looser structure than the latter. High magnification transmission electron microscope (TEM) images (Fig. 1d and 1 g) and SEM images (Fig. S1) indicate that, like in our previous work [29,30], the hierarchical structures of both materials are comprised of quite fine NFs.

From adsorption–desorption measurements of nitrogen, N_2, gas (Fig. S4), we estimated the SSAs to be 31.9 and 32.3 m^2/g for THS-T and THS-L powders, respectively. The isotherms exhibit type IV curves with H3 hysteresis loop, revealing the existence of irregular slit-pores, which probably stem from NF aggregation. Notably, these SSAs are far from the theoretical SSAs of the 1DL NFs that are – assuming a 5 Å thickness to the NFs – in the 1000 m^2/g range. We attribute the lower measured SSAs compared to the theoretical value to the dense self-assembly of structural building units (1D NFs) in THSs and the occupation of interfilamentous space by the intercalated ions such as TMA^+ and Li^+, both of which may prevent N_2 molecules from adsorbing to the internal surface of the NFs in THSs. This is not unique to our materials, but other 2D materials like MXenes as well [38–40]. It should also be noted that the low SSA obtained does not imply that there are few available adsorption sites in our THS adsorbents for water purification applications, since, as shown here, the intercalated ions surrounding the 1D NFs are capable of rapid exchange and release in aqueous solutions.

Thermogravimetric analysis, TGA, (Fig. 1j) of the THS-T and THS-L powders showed them to lose 23% and 13% of their weight when heated up to 700 °C, respectively. The main weight loss stage at ≤ 350 °C, corresponds to the release of interlayer water, hydration shells of intercalated ions, and/or a dehyroxylation process. The higher weight loss for THS-T can be attributed to the decomposition of TMA^+ cations during heating [26,30].

Zeta potential (ζ) measurements as a function of pH (Fig. 1k) indicate that the two sets of powders have similar zero charge points around pH 4.0. Like other titanate materials, their ζ become more negative with increasing pH due to the presence of Ti − O^- groups on the sorbent surface for pH > 4.0 [41].

2.2. Stability of THSs in aqueous solutions

Before investigating the adsorption behavior, it is important to evaluate the stability of the THSs in water in order to understand their dispersion and structural evolution. Since the THS powders are synthesized in high alkali conditions, and are thus known to be stable at high pH, our stability assessment was carried out mainly under neutral and acidic conditions. XRD patterns obtained after exposing the THS-T and THS-L powders to different pH solutions are shown in Fig. 2a and 2b, respectively. In both cases, the fundamental (1 1 0), (2 0 0) and (0 0 2) peaks are preserved for powders dispersed in deionized, DI, water. Under acidic conditions (Fig. 2a), the intensity of (0 2 0) diffraction peaks reduce significantly, with a low angle peak position shift to higher 2θ angles, implying that the order of THS-T along this stacking *b*-direction decreases and that the TMA^+ cations in the interlayer space were replaced by hydronium, H_3O^+ cations. The unchanged peak position of the (1 1 0)/(1 3 0) pair and (2 0 0) planes indicate that the THS-T's basic structural units, viz. 1DL NFs, are preserved after dispersion in water [26,29]. By contrast, the XRD patterns of the THS-L powders (Fig. 2b), appear to be undisturbed by the pH of the soaking solution. It is thus reasonable to conclude that replacing the TMA^+ with Li^+ results in better structural retention of the THSs. This conclusion is further confirmed by the morphological characterization of the dispersed samples (Fig. S5): the NFs of THS-T are rearranged to form thin films, while the flower-like hierarchical structure of THS-L remains unchanged. The structural evolution/instability of the THS-T powders most probably originate from the weak interlayer interaction between the TMA^+ ions and NFs. The importance of washing with LiCl on THS stability was first documented in Ref. [30].

Fig. 2c plots the weight of powders before and after soaking in the

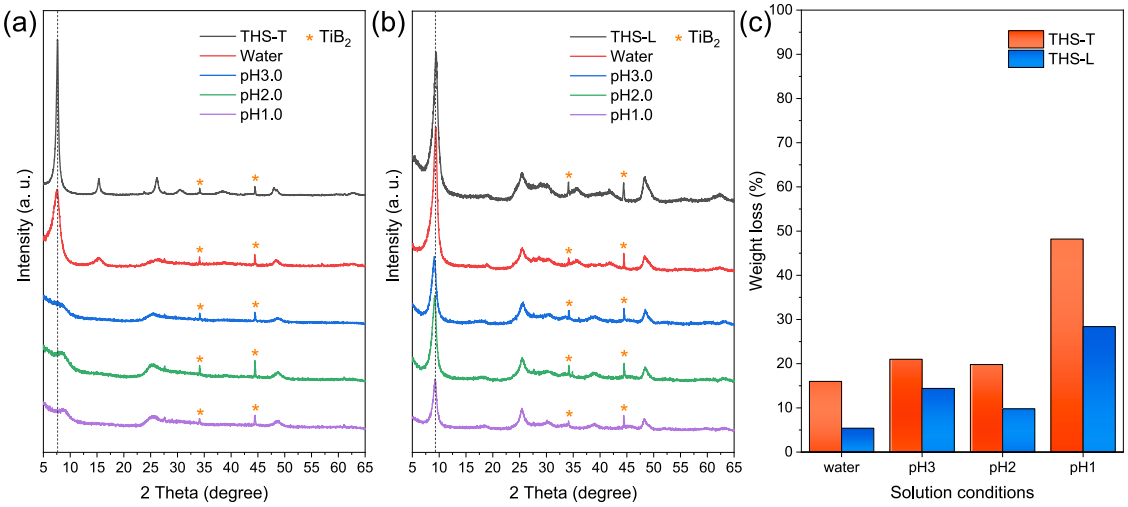

Fig. 2. Structural stability of THSs in low pH solutions. (a) XRD patterns for THS-T. (b) same as a, but for THS-L. (c) Weight loss of THS-T and THS-L powders dispersed in aqueous solutions under different pH conditions indicated on panel.

various pH solutions indicated on figure. The pH was varied using nitric, HNO_3 acid. At pH 2.0 and 3.0, the weight losses of the THS-T and THS-L powders are ≈ 20 wt% and 10 wt%, respectively. These values are comparable to losses in neutral DI water and are probably related to the release and exchange of intercalated ions. Soaking experiments under 0.1 M and 1 M nitric acid showed that the low pH leads to the dissolution of the THSs (Fig. 2c and Fig. S6). Based on these results, we confined our adsorption study to solutions with pH ≥ 2.0 and mostly 4.0 and 5.0.

2.3. Batch sorption experiments of THSs for actinide ion removal

Fig. 3a plots adsorption capacities of 1DL-based THSs for U(VI) as a function of contact time at pH 4.0. The adsorption equilibrium times of THS-T and THS-L powders are ≈ 4 h and ≈ 12 h, respectively. Although these rates are not too fast, nevertheless, 90% and 70% of the equilibrium adsorption capacities are reached - within 600 s - for the THS-T and THS-L powders, respectively. We ascribe the faster adsorption kinetics of the THS-T powders to the dispersion of the NFs in aqueous solutions. In the THS-L case, the more stable, and larger THSs present longer diffusion paths, slowing down the kinetics. To better understand the adsorption process, two kinetic models were employed to fit the adsorption data (Fig. S7) [42]. The fitting parameters are listed in Table S1. From the results it is obvious that a pseudo-second-order, PSO, kinetic model is a better fit and, not surprisingly, the THS-T kinetics are faster.

The adsorption behavior of another representative actinide ion, Th (IV), was also studied and the results (Fig. S8) showed that, here again, the THS-T powders provide faster adsorption kinetics. Moreover, it is quite interesting that the adsorption performances of the two 1DL-based THSs for Th(IV) and U(VI) are different. The adsorption capacity of THS-

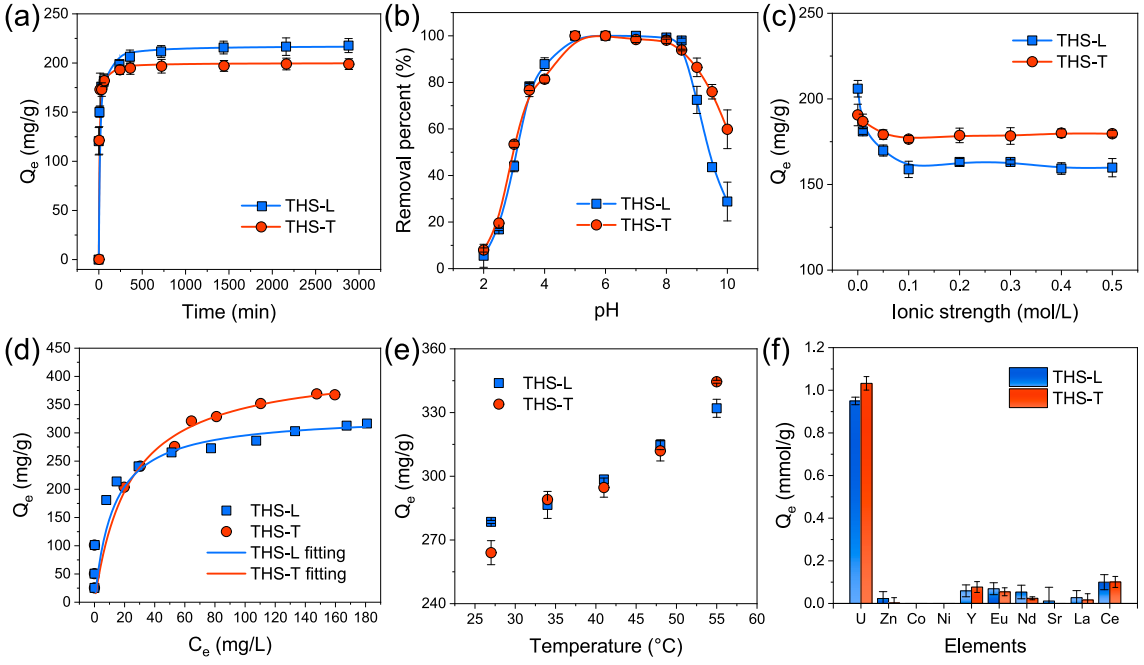

Fig. 3. U(VI) adsorption behavior of THS powders. (a) U(VI) removal kinetics of THS-L and THS-T. (b) Effect of pH on U(VI) removal. (c) Influence of ionic strength on U(VI) removal. (d) U(VI) adsorption isotherms of THS-L and THS-T powders. (e) Effect of temperature on adsorption of U(VI). (f) Selective adsorption experiments of U(VI) from solutions containing nine competitive metal cations.

T for Th(IV) is significantly higher than that of THS-L, while for U(VI) at pH 4.0, the adsorption capacity of THS-T is slightly lower than that of THS-L. It is noted that Th(IV) adsorption was performed at pH 2.5 (to avoid the hydrolysis of Th^{4+} ions), which corresponds to a high concentration of H^+ (~3.2 mmol/L) in the solution. A reasonable explanation is that the high concentration of H^+ plays the role of competing ion and inhibits the adsorption of Th(IV) onto THS-L, since the bonding strength of this kind of 1DL-based THSs for actinide ions is not as strong as that of THS-T (see below).

Fig. 3b shows that the THS-L and THS-T powders have similar U adsorption edges in the 2.5 to 4.0 pH range, where the rapid increase of U(VI) removal is consistent with the change of surface charge of 1DL-based THSs from positive to negative (see Fig. 1k). The positively charged surfaces, at low pHs, not surprisingly, repulse the cationic uranyl ion that, in turn, suppresses U(VI) uptake. When the solution pH is > 4.0, the negatively charged surface favors U(VI) adsorption, thereby resulting in up to almost 100% removal (Fig. 3b). In addition, it is well known that uranyl ions tend to hydrolyze and form positive species such as UO_2OH^+, $(UO_2)_2(OH)_2^{2+}$, and $(UO_2)_3(OH)_5^+$ with increases in solution pH [43,44], and neutral uranyl hydroxides may also precipitate in pH ranges of 6.0–8.0. These factors probably also contribute to the high removal rate of U. In contradistinction, the dramatic decrease in U(VI) removal at pH > 9.0 can be ascribed to the formation of anionic U(VI) species such as hydroxides and carbonate complexes [45,46], which are also unfavorable for adsorption on a negatively charged surface. Note that in the 4.0 to 8.0 pH range, THS-L has a slightly higher removal performance than THS-T, but its removal rate of U(VI) decreases more obviously under more acidic and alkaline conditions. This suggests that the adsorption of U by THS-L is more susceptible to environmental conditions.

To evaluate the influence of ionic strength on U(VI) removal, adsorption experiments were conducted at different concentrations of $NaClO_4$. The results are shown in Fig. 3c. With increasing salt concentration, the adsorption capacities of THS-L and THS-T decrease by 23% and 5%, respectively, reflecting that the latter has a higher affinity for U (VI) at high salinity.

In general, macroscopic adsorption mechanisms can be classified into two categories: inner-sphere and/or outer-sphere coordinations. In the former, the interaction is strong and is not affected by ionic strength. For the latter, it is mainly electrostatic attraction that belongs to weaker interactions where adsorbed ions can be readily exchanged in concentrated salts, resulting in significant decreases in uptake capacities. Based on the results shown in Fig. 3c, it is reasonable to conclude that the adsorption of U(VI) on THS-T is dominated by the stable inner-sphere coordination, while both inner- and outer-sphere complexes are formed on the THS-L surfaces. This conclusion can also explain why the adsorption performance of THS-L for Th(IV) is significantly decreased compared with that of THS-T in the presence of a high concentration of H_3O^+, as described previously.

Fig. 3d shows adsorption isotherms of 1DL-based THSs. With increases of U(VI) concentration, the uptake capacities increase accordingly. The isotherms were fitted assuming the Langmuir and Freundlich models (see Supplementary Material). Fitting parameters are summarized in Table S2. The former resulted in higher correlation coefficients, suggesting that this homogeneous adsorption model can describe the adsorption quite well. The maximum sorption capacities of THS-T and THS-L, at pH 4.0, are calculated to be 424 mg/g and 332 mg/g, respectively, outperforming most of the state-of-the art inorganic adsorbent materials (Table S3) including GO [47,48], MXene [49–51], titanate [23–25], metal oxides [15,52], layered metal sulfides [53,54], and others.

The effects of temperature on U(VI) adsorption are plotted in Fig. 3e, where it is obvious that higher temperatures favor U(VI) adsorption by both materials. When the data shown in Fig. 3e are replotted as Van't Hoff plots (Fig. S9), fitting the latter results in the calculated parameters listed in Table S4. From these results it is obvious that the enthalpy change (ΔH) is positive. Said otherwise, the adsorption process is endothermic [55–57]. Not surprisingly, the positive entropic change, ΔS, is what renders △G negative, leading to spontaneous adsorption.

To evaluate the ion selectivity of our materials, adsorption experiments were conducted in mixed solutions containing 0.5 mmol/L U(VI) and nine other cations, including transition metal and rare earth cations (see Supplementary Material). As shown in Fig. 3f, the uptake capacity of THS-L and THS-T for U(VI) is as high as 0.95 mmol/g (226 mg/g) and 1.03 mmol/g (246 mg/g), respectively. The adsorption capacities for the other competing cations is < 0.10 mmol/g. It follows that competing ions have little influence on U(VI) adsorption by our THSs. To further quantify our adsorbents' selectivity, the selectivity coefficient ($S_{U/M}$), defined as the ratio of distribution coefficients of U(VI) and competing ions, was extracted and compared. Table S5 lists the results – together with many others in the literature – that show that $S_{U/M}$ of THS-L and THS-T are > 30 and 50, respectively, demonstrating high selectivity values. Here again these values are significantly higher than other inorganic adsorbents such as MXene [49,50], graphene oxide [58], functionalized mesoporous silica [59], mesoporous carbon [60], and metal oxides [61]. These findings apparently indicate that 1DL-based THSs, especially THS-T, have quite attractive application potential in the selective separation of U.

In addition, THS-T and THS-L were regenerated using eluents containing 0.01 M HCl and 1 M tetramethylammonium chloride or 1 M LiCl in order to assess their reusability. According to the results shown in Fig. S10, U(VI) adsorption decline slowly with increasing numbers of cycles. For example, the U(VI) removal rate of THS-T remained at 82% after the third cycle, which is about 9% lower than that of the fresh adsorbent. We attribute the decline in the adsorption performance to the occupation of some adsorption sites by U(VI) in the regeneration process due to their strong binding. Nevertheless, after five sorption/desorption cycles, THS-T and THS-L still exhibited high U(VI) uptake capacities of 185 mg/g and 163 mg/g, with corresponding regeneration efficiency of 81% and 75%, respectively. A comparison of removal and regeneration efficiency between our THS materials and other reported adsorbents is summarized in Table S6. The results show that THS-T and THS-L have acceptable reusability in terms of regeneration efficiency and adsorption capacity.

2.4. U removal from simulated radioactive wastewater by THSs

On the basis of batch adsorption experiments, we further evaluated the performance of our THSs for U(VI) removal in the field of water purification. The bivalent Ca^{2+} and Mg^{2+} are ubiquitous, and sometimes at high concentrations in natural water and environmental wastewater have a significant negative impact on the removal efficiency of heavy metal ions [11]. Therefore, the selective removal ability of 1DL-based THSs for U(VI) from water with different concentrations of Ca^{2+} and Mg^{2+} was evaluated and compared with a common commercial ion exchange resin (IR 120). The results (Fig. 4a and 4b) show that the removal rates of U(VI) by THS-T and THS-L only slightly decrease with the increase of the concentration of competing ions; while for the non-specific electrostatic adsorbed IR 120, U(VI) removal percent is suppressed to < 15% in the presence of 4 mmol/L Ca^{2+} or Mg^{2+}. At a relatively high Ca/U and Mg/U molar ratios of 1523 (128 mmol/L Ca^{2+}/Mg^{2+}), THS-T remove 81.5% and 90.7% U(VI), respectively. The corresponding distribution coefficients (K_d) are 2.2×10^4 and 5.4×10^4 mL/g, respectively. For THS-L, at the same Ca/U and Mg/U ratios, the removal rates are 80.8% and 76.5%, respectively. The corresponding K_d values are 2.1×10^4 and 1.6×10^4 mL/g, respectively. Higher K_d values implies a stronger binding affinity between adsorbate and adsorbent and materials with $K_d > 5 \times 10^3$ mL/g are generally considered to be excellent adsorbents [62,63]. Based on that criteria it is reasonable to conclude that our THS powders exhibit outstanding enrichment selectivity for U(VI) against Ca^{2+} and Mg^{2+} competing cations.

Further purification experiments dealing with simulated U-

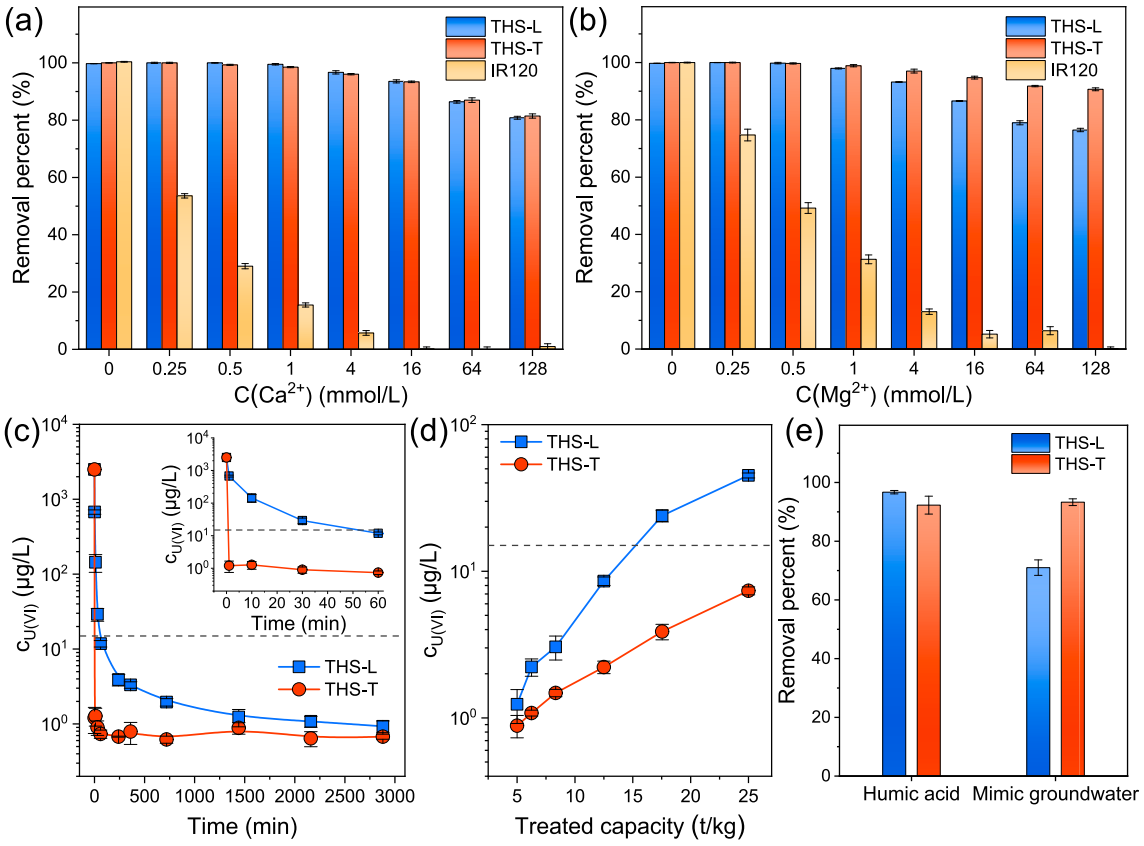

Fig. 4. Practical application of THS-L and THS-T for the purification of U-containing simulated radioactive wastewater. (a) U(VI) uptake efficiency onto THS-L, THS-T and ion-exchange resin IR 120 as a function of concentrations of Ca(II). (b) same as (a) but for Mg(II). (c-d) Evaluation of purification performance of THS-L and THS-T for U(VI) elimination from simulated U-contaminated potable water. Dashed horizontal lines in (c) and (d) is the interim standard (15 μg/L) of U concentration in drinking water recommended by World Health Organization. (e) Influence of environmental media (humic acid and synthetic groundwater) on U(VI) elimination by THS-L and THS-T.

contaminated potable water containing 60-fold (molar ratio) Ca^{2+}, 100-fold Mg^{2+} and 200-fold Na^{+} show that the THS-T powders can reduce the concentration of U(VI) from 2,500 μg/L to around 1 μg/L in one minute and eventually to 0.6 μg/L (Fig. 4c). This value is far below the drinking water interim standard (15 μg/L) of U-concentration recommended by the World Health Organization, WHO. Despite the fact the THS-L's U-removal kinetics are slower than those of THS-T (Fig. 4c), nevertheless, the U(VI) concentration drops from 2500 μg/L to < 15 μg/L in 1 h (Fig. 4c). The residual concentrations, at equilibrium, are as low as 0.9 μg/L. The K_d values extracted from the purification experiments -2.1×10^7 and 1.0×10^7 mL/g for THS-T and THS-L powders, respectively – are amongst the highest reported U adsorbents.

Moreover, THSs have shown both remarkable treatment capacity and high removal efficiency for U-contaminated wastewater. Fig. 4d indicates that 1 kg THS-T or THS-L powders can treat >25 tons and about 15 tons of U-contaminated potable water without exceeding the limit WHO concentration standard. The corresponding U(VI) removal rates are higher than 99.7% and 99.4%, respectively. The THSs can also efficiently remove U in other environmental media including humic acid and simulated groundwater, as shown in Fig. 4e. The above results firmly demonstrate that our 1DL-based THSs, especially THS-T, have promising application prospects in the purification of low and medium concentration U-containing drinking water and environmental wastewater.

2.5. Uranium elimination mechanism by 1DL-based THSs

To better understand U speciation and underlying removal mechanisms, XRD patterns, SEM images, X-ray absorption fine structure (XAFS) and XPS of U-adsorbed samples were acquired and carefully examined. The *d*-spacing of THS-L increased from 9.3 Å to 11.7 Å after U (VI) adsorption (Fig. S11), clearly indicating the successful intercalation of uranyl ion into the inter-filament space. The shift is observed in 4.0 and 5.0 pH solutions. In the THS-T case, the (0 2 0) peak almost disappears (Fig. S11), indicating that the order along the stacking direction is mostly lost. Interestingly, the *d*-spacing does not change for TMA^{+} intercalated THS-T after U(VI) adsorption.

High resolution XPS spectra in C1s and N1s regions are shown in Fig. S12a and S12b, respectively. After U-adsorption, the N-signal disappears (Fig. S12b). Concomitantly, a strong U signal is detected for both powders (Fig. S13), suggesting that the guest intercalated ions are fully exchanged with uranyl ions. Thus, at the initial stages of adsorption, Li^{+} or TMA^{+} in the both THSs are replaced by uranyl ions through ion exchange.

At the SEM level (Fig. S14), the morphologies of the THS-L particles retained their shape whereas those of their THS-T counterparts collapsed after U adsorption. These results are fully consistent with the results of our stability evaluation for the two materials in water (Fig S5). It is reasonable to assume at this time that the structural rearrangement of the NFs exposes more THS-T active sites to fully interact with U(VI) in aqueous solution in quite short times, resulting in outstanding adsorption capacity and ultra-fast water purification performance.

The U L_3 edge XAFS spectra of adsorbed samples and references (UO_2, uranyl nitrate hexahydrate, UNH-solid, and its aqueous solution, UNH-aq) were collected to identify the uranium speciation. The X-ray absorption near edge structure (XANES) white line shapes and peak positions for all U-loaded samples were consistent with the reference of uranyl ion in aqueous solutions (Fig. 5a), indicating the U is mainly

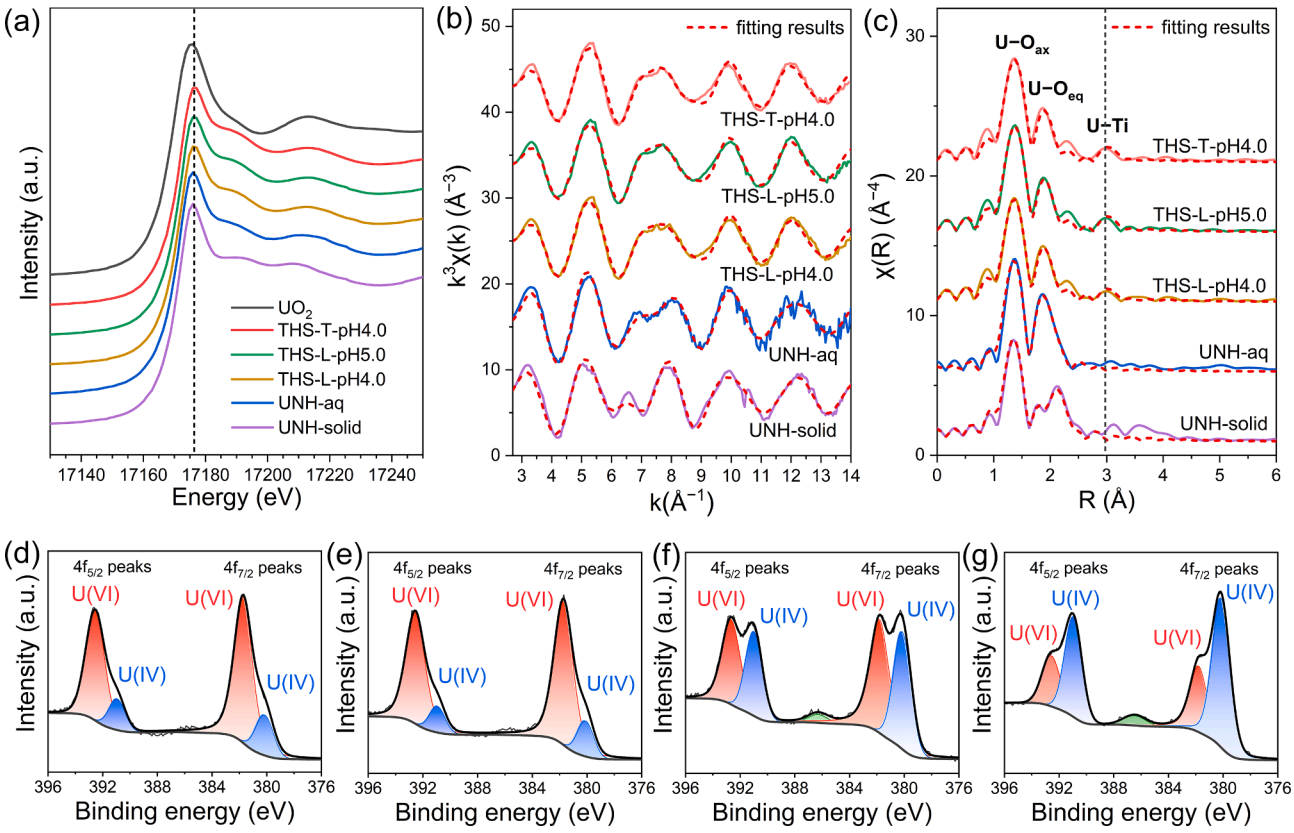

Fig. 5. Spectral analysis of U-speciation by XAFS and XPS techniques. (a) U L_3 edge XANES spectra of U-containing THS powders and references. (b) U L_3 edge k^3-weighted EXAFS spectra (solid lines) and the best theoretical fitting results (dotted lines). (c) Corresponding nonphase shift corrected Fourier transforms. (d-g) U 4f region XPS spectra and fitting results of U-loaded 1DL-based THSs prepared under aerobic (air) and anaerobic (Ar) conditions. (d) THS-L, adsorption in air; (e) THS-T, adsorption in air; (f) THS-L, adsorption in Ar; (g) THS-T, adsorption in Ar.

adsorbed in the U(VI) oxidation state. The local U coordination environments were further probed by analysis and fitting of the k^3-weighted extended XAFS (EXAFS) data (Fig. 5b) and their Fourier transforms, FTs (Fig. 5c). The shape, and amplitude, of the oscillation periods of the three samples in the 6–13 $Å^{-1}$ k-space range are similar to each other, but notably different from the reference, UNH-aq, (Fig. 5b), reflecting changes in the equatorial coordination of the uranyl ions.

The FT fitting results of U-adsorbed samples (Fig. 5c and Table S7) suggest that there are two O atoms at 1.78–1.79 Å and five O atoms at 2.37 Å, which can be ascribed to the axial uranyl O atoms (U − O_{ax}) and equatorial coordinated O atoms (U − O_{eq}), respectively. The average U − O_{eq} distance of U in adsorbents is ≈ 0.05 Å less than that of UNH-aq (2.42 Å), which confirms the strong coordination interaction of 1DL-based THSs for uranyl ions. More importantly, a U − Ti interaction at 3.43–3.44 Å is fitted as the second equatorial shell of U(VI), which is consistent with the EXAFS results (3.37–3.54 Å) of U-adsorbed titanates and Ti_2CT_x MXene [17,64]. The presence of a U − Ti interaction with the aforementioned distance also reflects that the uranyl ion may bond with the two adjacent O atoms around the Ti atoms in both THS-L and THS-T to form a stable bidentate inner-sphere coordination complex. Since the first equatorial shell of U(VI) with a bidentate fashion is usually comprised of two bonded O atoms (U − O_b) and three coordinated water (U − O_w) [65–68], an estimate has been conducted based on two U − O_b with distances of 2.29 Å and 2.33 Å extracted from a $BaUO_2TiO_4$ crystal structure and U − O_w with distance of 2.42 Å (U − O_{eq} of hydrated uranyl ion, Table S7). The calculated average distance of U − O_{eq} (2.38 Å) is quite close to the XAFS fitting result (2.37 Å), once again demonstrating the rationality of assuming a bidentate coordination configuration between the uranyl ions and the THSs powders. Additionally, at pH 4.0, the THS-L samples have a smaller coordination number (CN) of U − Ti than their THS-T counterparts (Table S7). This implies a relatively reduced contribution of inner-sphere coordination adsorption, which is consistent with the experimental results of ionic strength (Fig. 3c). As the pH increased from 4.0 to 5.0, the CN of U-Ti for THS-L increased from 0.6 to around 1.1, suggesting that higher pHs are more favorable for the formation of stable uranyl surface complexes.

Fitting of high resolution XPS spectra in the U 4f region further reveals that besides the main U(VI) $U4f_{7/2}$ and $U4f_{5/2}$ peaks centered at 381.8 and 392.6 eV [64], a U(IV) component – centered at 380.2 and 391.0 eV – with a fraction of about 15% also exists in U-adsorbed THS-L and THS-T samples (Fig. 5d and 5e). Since this adsorption experiment was carried out under ambient air, with no special protection, it is not surprising that ≈ 15% of the adsorbed U species is in a lower oxidation states. Concomitant by the adsorption and reduction of U, it is found that the Ti 2p and O 1 s peaks of the 1DL-based THSs shift to higher binding energy, BE, regions (Fig. S15 and S16), with the BE of THS-T changing more. The literature reveals that the oxygen vacancies in TiO_{2-x} can provide high chemical activity to trap U(VI) in the defective sites, which in turn lowers the BEs of U [14]. Our previous studies reported the presence of Ti in an unsaturated oxidation state and the presence of sufficient defects in 1DL-based NFs [26]. Combined with the findings of this study, it can be deduced that these two factors will enhance the adsorption affinity of both powders and achieve partial U(VI) reduction fixation, thus achieving high selectivity and efficient removal of U.

Adsorption experiments under anaerobic conditions were also carried out to further verify the above conclusions. The XPS results (Fig. 5f and 5 g) show that under Ar protection, the fractions of U(IV) in THS-T and THS-L powders increase significantly to 67.6% and 42.9%, respectively. Although XPS is a surface probing technique, these results clearly show that the THS-T powder possess more reductive active sites than

THS-L. It is this capability that we invoke to explain the superior U selectivity and removal capability of THS-T compared the THS-L.

3. Conclusions

In summary, two 1DL-based titanate hierarchical structures (THS-T and THS-L) with TMA^+ and Li^+ cations in the interfilamentous space were synthesized and deployed for the removal of actinides from aqueous solutions. It is found that the adsorption of U(VI) onto both THSs is a spontaneous and entropy-increasing ion-exchange process, and the adsorption kinetics and isotherms can be well described by POS and Langmuir models, respectively. Compared with THS-L, the disaggregation of THS-T powders in water results in faster adsorption kinetics, higher adsorption capacities, better U-selectivity and more tolerance in the presence of environmental interferents. Further spectroscopic analyses unveil that the efficient U adsorption by the THS powders is realized through complex mechanisms that includes inner-sphere complexation, reduction fixation and electrostatic interactions.

There have been many studies on materials for the removal of actinide and other heavy metal cations from water. What renders this work unique and impactful are three factors. The first two include the near record adsorption capacity coupled with near record selectivity coefficients of our THS adsorbents. The most impactful, however, has to be the ease and simplicity of making kilogram scale 1DL powders starting with relatively inexpensive, ubiquitous, non-toxic, earth abundant precursors powders such as TiB_2, TiC, TiN among others. From the perspective of practical applications, our THS adsorbents show excellent removal efficiency for U(VI) in the wide pH range of 3.0–10.0, and their performance is hardly affected by high salinity and/or complex environmental media. As for the treatment of U-contaminated drinking water, THS-T exhibits ultra-fast water purification efficiency (3 orders of magnitude reduction of U-concentration in 60 s) and ultra-high purification capacity (>25 ton/kg of adsorbents), and the residual concentration of U(VI) in the treated water is far below the WHO drinking water standard. In addition, our THSs retain acceptable regeneration efficiency and high U(VI) removal capacities after five cycles. As a result, we strongly believe that our THSs materials have broad application prospects in the enrichment of radionuclides and other heavy metal ions, purification of drinking water, and elimination of environmental pollutants with high oxidation states.

Declaration of Competing Interest

The authors declare that they have no known competing financial interests or personal relationships that could have appeared to influence the work reported in this paper.

Data availability

Data will be made available on request.

Acknowledgements

This work was supported by the National Science Foundation, (DMR-2211319). This work was also supported by the National Science Fund for Distinguished Young Scholars (Grant No. 21925603), the National Natural Science Foundation of China (Grant Nos. 22176190, U20B2019), and Youth Innovation Promotion Association CAS (2021010). We are grateful to the staff of Beijing Synchrotron Radiation Facility (BSRF) for EXAFS and XANES measurement.

Appendix A. Supplementary data

Supplementary data to this article can be found online at https://doi.org/10.1016/j.cej.2023.145635.

References

[1] X.Q. Xie, C. Chen, N. Zhang, Z.R. Tang, J.J. Jiang, Y.J. Xu, Microstructure and surface control of MXene films for water purification, Nat. Sustain. 2 (9) (2019) 856–862, https://doi.org/10.1038/s41893-019-0373-4.
[2] M.S. Mauter, I. Zucker, F. Perreault, J.R. Werber, J.H. Kim, M. Elimelech, The role of nanotechnology in tackling global water challenges, Nat. Sustain. 1 (4) (2018) 166–175, https://doi.org/10.1038/s41893-018-0046-8.
[3] X.X. Wang, L. Chen, L. Wang, Q.H. Fan, D.Q. Pan, J.X. Li, F.T. Chi, Y. Xie, S.J. Yu, C.L. Xiao, F. Luo, J. Wang, X.L. Wang, C.L. Chen, W.S. Wu, W.Q. Shi, S. Wang, X. K. Wang, Synthesis of novel nanomaterials and their application in efficient removal of radionuclides, Sci. China. Chem. 62 (8) (2019) 933–967, https://doi.org/10.1007/s11426-019-9492-4.
[4] V.K.K. Upadhyayula, S.G. Deng, M.C. Mitchell, G.B. Smith, Application of carbon nanotube technology for removal of contaminants in drinking water: A review, Sci. Total Environ. 408 (1) (2009) 1–13, https://doi.org/10.1016/j.scitotenv.2009.09.027.
[5] V.K. Gupta, R. Kumar, A. Nayak, T.A. Saleh, M.A. Barakat, Adsorptive removal of dyes from aqueous solution onto carbon nanotubes: A review, Adv. Colloid Interface Sci. 193 (2013) 24–34, https://doi.org/10.1016/j.cis.2013.03.003.
[6] J. Zhao, Z.Y. Wang, J.C. White, B.S. Xing, Graphene in the Aquatic Environment: Adsorption, Dispersion, Toxicity and Transformation, Environ. Sci. Tech. 48 (17) (2014) 9995–10009, https://doi.org/10.1021/es5022679.
[7] J. Wang, Z.M. Chen, B.L. Chen, Adsorption of Polycyclic Aromatic Hydrocarbons by Graphene and Graphene Oxide Nanosheets, Environ. Sci. Tech. 48 (9) (2014) 4817–4825, https://doi.org/10.1021/es405227u.
[8] M. Naguib, M. Kurtoglu, V. Presser, J. Lu, J.J. Niu, M. Heon, L. Hultman, Y. Gogotsi, M.W. Barsoum, Two-Dimensional Nanocrystals Produced by Exfoliation of Ti_3AlC_2, Adv. Mater. 23 (37) (2011) 4248–4253, https://doi.org/10.1002/adma.201102306.
[9] M. Ghidiu, M.R. Lukatskaya, M.Q. Zhao, Y. Gogotsi, M.W. Barsoum, Conductive two-dimensional titanium carbide 'clay' with high volumetric capacitance, Nature 516 (7529) (2014) 78–81, https://doi.org/10.1038/nature13970.
[10] M. Naguib, O. Mashtalir, J. Carle, V. Presser, J. Lu, L. Hultman, Y. Gogotsi, M. W. Barsoum, Two-Dimensional Transition Metal Carbides, ACS Nano 6 (2) (2012) 1322–1331, https://doi.org/10.1021/nn204153h.
[11] Q.M. Peng, J.X. Guo, Q.R. Zhang, J.Y. Xiang, B.Z. Liu, A.G. Zhou, R.P. Liu, Y. J. Tian, Unique Lead Adsorption Behavior of Activated Hydroxyl Group in Two-Dimensional Titanium Carbide, J. Am. Chem. Soc. 136 (11) (2014) 4113–4116, https://doi.org/10.1021/ja500506k.
[12] K. Rasool, R.P. Pandey, P.A. Rasheed, S. Buczek, Y. Gogotsi, K.A. Mahmoud, Water treatment and environmental remediation applications of two-dimensional metal carbides (MXenes), Mater. Today 30 (2019) 80–102, https://doi.org/10.1016/j.mattod.2019.05.017.
[13] J. Li, X.X. Wang, G.X. Zhao, C.L. Chen, Z.F. Chai, A. Alsaedi, T. Hayat, X.K. Wang, Metal-organic framework-based materials: superior adsorbents for the capture of toxic and radioactive metal ions, Chem. Soc. Rev. 47 (7) (2018) 2322–2356, https://doi.org/10.1039/c7cs00543a.
[14] S.A. Song, S.Y. Huang, R. Zhang, Z.S. Chen, T. Wen, S.H. Wang, T. Hayat, A. Alsaedi, X.K. Wang, Simultaneous removal of U(VI) and humic acid on defective TiO_{2-x} investigated by batch and spectroscopy techniques, Chem. Eng. J. 325 (2017) 576–587, https://doi.org/10.1016/j.cej.2017.05.125.
[15] M.C. Kimling, N. Scales, T.L. Hanley, R.A. Caruso, Uranyl-Sorption Properties of Amorphous and Crystalline TiO_2/ZrO_2 Millimeter-Sized Hierarchically Porous Beads, Environ. Sci. Tech. 46 (14) (2012) 7913–7920, https://doi.org/10.1021/es3011157.
[16] M.J. Comarmond, T.E. Payne, J.J. Harrison, S. Thiruvoth, H.K. Wong, R. D. Aughterson, G.R. Lumpkin, K. Muller, H. Foerstendorf, Uranium Sorption on Various Forms of Titanium Dioxide - Influence of Surface Area, Surface Charge, and Impurities, Environ. Sci. Tech. 45 (13) (2011) 5536–5542, https://doi.org/10.1021/es201046x.
[17] M.C. Duff, D.B. Hunter, D.T. Hobbs, S.D. Fink, Z. Dai, J.P. Bradley, Mechanisms of strontium and uranium removal from high-level radioactive waste simulant solutions by the sorbent monosodium titanate, Environ. Sci. Tech. 38 (19) (2004) 5201–5207, https://doi.org/10.1021/es035415+.
[18] G.D. Sheng, S.T. Yang, D.L. Zhao, J. Sheng, X.K. Wang, Adsorption of Eu(III) on titanate nanotubes studied by a combination of batch and EXAFS technique, Sci. China Chem. 55 (1) (2012) 182–194, https://doi.org/10.1007/s11426-011-4370-3.
[19] G.D. Sheng, B.W. Hu, Role of solution chemistry on the trapping of radionuclide Th (IV) using titanate nanotubes as an efficient adsorbent, J. Radioanal. Nucl. Chem. 298 (1) (2013) 455–464, https://doi.org/10.1007/s10967-012-2389-3.
[20] P. Zhang, L. Wang, L.Y. Yuan, J.H. Lan, Z.F. Chai, W.Q. Shi, Sorption of Eu(III) on MXene-derived titanate structures: The effect of nano-confined space, Chem. Eng. J. 370 (2019) 1200–1209, https://doi.org/10.1016/j.cej.2019.03.286.
[21] D.J. Yang, S. Sarina, H.Y. Zhu, H.W. Liu, Z.F. Zheng, M.X. Xie, S.V. Smith, S. Komarneni, Capture of Radioactive Cesium and Iodide Ions from Water by Using Titanate Nanofibers and Nanotubes, Angew. Chem. Int. Ed. 50 (45) (2011) 10594–10598, https://doi.org/10.1002/anie.201103286.
[22] L. Yin, S. Song, X.X. Wang, F.L. Niu, R. Ma, S.J. Yu, T. Wen, Y.T. Chen, T. Hayat, A. Alsaedi, X.K. Wang, Rationally designed core-shell and yolk-shell magnetic titanate nanosheets for efficient U(VI) adsorption performance, Environ. Pollut. 238 (2018) 725–738, https://doi.org/10.1016/j.envpol.2018.03.092.
[23] W. Liu, X. Zhao, T. Wang, D.Y. Zhao, J.R. Ni, Adsorption of U(VI) by multilayer titanate nanotubes: Effects of inorganic cations, carbonate and natural organic

matter, Chem. Eng. J. 286 (2016) 427–435, https://doi.org/10.1016/j.cej.2015.10.094.
[24] F. Yuan, C.F. Wu, Y.W. Cai, L.J. Zhang, J.Q. Wang, L.H. Chen, X.K. Wang, S. T. Yang, S.A. Wang, Synthesis of phytic acid-decorated titanate nanotubes for high efficient and high selective removal of U(VI), Chem. Eng. J. 322 (2017) 353–365, https://doi.org/10.1016/j.cej.2017.03.156.
[25] J. Duan, H.D. Ji, T.Y. Xu, F. Pan, X.N. Liu, W. Liu, D.Y. Zhao, Simultaneous adsorption of uranium(VI) and 2-chlorophenol by activated carbon fiber supported/modified titanate nanotubes (TNTs/ACF): Effectiveness and synergistic effects, Chem. Eng. J. 406 (2021), 126752, https://doi.org/10.1016/j.cej.2020.126752.
[26] H.O. Badr, T. El-Melegy, M. Carey, V. Natu, M.Q. Hassig, C. Johnson, Q. Qian, C. Y. Li, K. Kushnir, E. Colin-Ulloa, L.V. Titova, J.L. Martin, R.L. Grimm, R. Pai, V. Kalra, A. Karmakar, A. Ruffino, S. Masiuk, K. Liang, M. Naguib, O. Wilson, A. Magenau, K. Montazeri, Y.C. Zhu, H. Cheng, T. Torita, M. Koyanagi, A. Yanagimachi, T. Ouisse, M. Barbier, F. Wilhelm, A. Rogalev, J. Bjork, P.O. A. Persson, J. Rosen, Y.J. Hu, M.W. Barsoum, Bottom-up, scalable synthesis of anatase nanofilament-based two-dimensional titanium carbo-oxide flakes, Mater. Today 54 (2022) 8–17, https://doi.org/10.1016/j.mattod.2021.10.033.
[27] H.O. Badr, K. Montazeri, T. El-Melegy, V. Natu, M. Carey, R. Gawas, P. Phan, Q. Qian, C.Y. Li, U. Wiedwald, M. Farle, E. Colin-Ulloa, L.V. Titova, M. Currie, T. Ouisse, M. Barbier, A. Rogalev, F. Wilhelm, M. Hans, J.M. Schneider, C. Tandoc, Y.J. Hu, J. Snyder, M.W. Barsoum, Scalable, inexpensive, one-pot, facile synthesis of crystalline two-dimensional birnessite flakes, Matter 5 (7) (2022) 2365–2381, https://doi.org/10.1016/j.matt.2022.05.038.
[28] W. Zheng, J. Halim, L. Yang, H.O. Badr, Z.M. Sun, P.O.A. Persson, J. Rosen, M. W. Barsoum, MXene//MnO_2 Asymmetric Supercapacitors with High Voltages and High Energy Densities, Batteries Supercaps 5 (10) (2022) e02200151, https://doi.org/10.1002/batt.202200151.
[29] H.O. Badr, F. Lagunas, D.E. Autrey, J. Cope, T. Kono, T. Torita, R.F. Klie, Y.J. Hu, M.W. Barsoum, On the structure of one-dimensional TiO_2 lepidocrocite, Matter 6 (1) (2023) 128–141, https://doi.org/10.1016/j.matt.2022.10.015.
[30] H.O. Badr, J. Cope, T. Kono, T. Torito, A. Karmakar, F. Lagunas, E. Castiel, R.F. Klie, M.W. Barsoum, Titanium Oxide-based 1D Nanofilaments, 2D Sheets, and Mesoporous Particles: Synthesis, Characterization, and Ion Intercalation, Matter 6 (2023), accepted, https://doi.org/10.1016/j.matt.2023.07.022.
[31] E. Colin-Ulloa, J.L. Martin, R.J. Hanna, M.H. Frasch, R.R. Ramthun, H.O. Badr, J. R. Uzarski, M.W. Barsoum, R.L. Grimm, L.V. Titova, Electronic Structure of 1D Lepidocrocite TiO_2 as Revealed by Optical Absorption and Photoelectron Spectroscopy, J. Phys. Chem. C 127 (15) (2023) 7275–7283, https://doi.org/10.1021/acs.jpcc.2c06719.
[32] N. Cardoza, H.O. Badr, R. Pereira, M.W. Barsoum, V. Kalra, T. Titania Lepidocrocite-based, Nanofilaments and Their Polysulfide Anchoring Capabilities in Lithium Sulfur Batteries, ACS Appl. Mater. Interfaces (2023) accepted.
[33] K. Sudhakar, A. Karmakar, H.O. Badr, T. El-Melegy, M.Q. Hassig, M. Carey, S. Masiuk, L. Wu, Q. Qian, T. Kono, C.Y. Li, M.W. Barsoum, One-dimensional, titania-based lepidocrocite nanofilaments and their self-assembly, Matter (2023), in press, https://doi.org/10.1016/j.matt.2023.06.006.
[34] T. Xiong, Q.C. Li, J. Liao, Y. Zhang, W.K. Zhu, Highly enhanced adsorption performance to uranium(VI) by facile synthesized hydroxyapatite aerogel, J. Hazard. Mater. 423 (2022), 127184, https://doi.org/10.1016/j.jhazmat.2021.127184.
[35] X. Li, Z.R. Liu, M. Huang, Purification of uranium-containing wastewater by adsorption: a review of research on resin materials, J. Radioanal. Nucl. Chem. 331 (7) (2022) 3043–3075, https://doi.org/10.1007/s10967-022-08370-6.
[36] J. Yu, C.H. Yu, W.K. Zhu, G.Q. He, Y.X. Wei, J. Zhou, Hydrous titanium oxide and bayberry tannin co-immobilized nano collagen fibrils for uranium extraction from seawater and recovery from nuclear wastewater, Chemosphere 286 (2022), 131626, https://doi.org/10.1016/j.chemosphere.2021.131626.
[37] F.F. Li, W.R. Cui, W. Jiang, C.R. Zhang, R.P. Liang, J.D. Qiu, Stable sp^2 carbon-conjugated covalent organic framework for detection and efficient adsorption of uranium from radioactive wastewater, J. Hazard. Mater. 392 (2020), 122333, https://doi.org/10.1016/j.jhazmat.2020.122333.
[38] P.A. Maughan, L. Bouscarrat, V.R. Seymour, S.Q. Shao, S.J. Haigh, R. Dawson, N. Tapia-Ruiz, N. Bimbo, Pillared Mo_2TiC_2 MXene for high-power and long-life lithium and sodium-ion batteries, Nanoscale Adv. 3 (11) (2021) 3145–3158, https://doi.org/10.1039/d1na00081k.
[39] M. Naguib, J. Come, B. Dyatkin, V. Presser, P.L. Taberna, P. Simon, M.W. Barsoum, Y. Gogotsi, MXene: a promising transition metal carbide anode for lithium-ion batteries, Electrochem. Commun. 16 (1) (2012) 61–64, https://doi.org/10.1016/j.elecom.2012.01.002.
[40] L. Li, M.Y. Zhang, X.T. Zhang, Z.G. Zhang, New Ti_3C_2 aerogel as promising negative electrode materials for asymmetric supercapacitors, J. Power Sources 364 (2017) 234–241, https://doi.org/10.1016/j.jpowsour.2017.08.029.
[41] X. Zhao, P.H. Du, Z.Q. Cai, T. Wang, J. Fu, W. Liu, Photocatalysis of bisphenol A by an easy-settling titania/titanate composite: Effects of water chemistry factors, degradation pathway and theoretical calculation, Environ. Pollut. 232 (2018) 580–590, https://doi.org/10.1016/j.envpol.2017.09.094.
[42] S. Azizian, Kinetic models of sorption: a theoretical analysis, J. Colloid Interf. Sci. 276 (1) (2004) 47–52, https://doi.org/10.1016/j.jcis.2004.03.048.
[43] L.P. Lingamdinne, J.S. Choi, G.K.R. Angaru, R.R. Karri, J.K. Yang, Y.Y. Chang, J. R. Koduru, Magnetic-watermelon rinds biochar for uranium-contaminated water treatment using an electromagnetic semi-batch column with removal mechanistic investigations, Chemosphere 286 (2022), 131776, https://doi.org/10.1016/j.chemosphere.2021.131776.
[44] L.P. Lingamdinne, V.R. Lebaka, J.R. Koduru, Y.Y. Chang, Insights into manganese ferrite anchored graphene oxide to remove Cd(II) and U(VI) via batch and semi-batch columns and its potential antibacterial applications, Chemosphere 310 (2023), 136888, https://doi.org/10.1016/j.chemosphere.2022.136888.
[45] K. Brix, S. Baur, A. Haben, R. Kautenburger, Building the bridge between U(VI) and Ca-bentonite - Influence of concentration, ionic strength, pH, clay composition and competing ions, Chemosphere 285 (2021), 131445, https://doi.org/10.1016/j.chemosphere.2021.131445.
[46] M. Wazne, G.P. Korfiatis, X.G. Meng, Carbonate effects on hexavalent uranium adsorption by iron oxyhydroxide, Environ. Sci. Tech. 37 (16) (2003) 3619–3624, https://doi.org/10.1021/es034166m.
[47] Y.B. Sun, D.D. Shao, C.L. Chen, S.B. Yang, X.K. Wang, Highly Efficient Enrichment of Radionuclides on Graphene Oxide-Supported Polyaniline, Environ. Sci. Tech. 47 (17) (2013) 9904–9910, https://doi.org/10.1021/es401174n.
[48] Z.J. Li, F. Chen, L.Y. Yuan, Y.L. Liu, Y.L. Zhao, Z.F. Chai, W.Q. Shi, Uranium(VI) adsorption on graphene oxide nanosheets from aqueous solutions, Chem. Eng. J. 210 (2012) 539–546, https://doi.org/10.1016/j.cej.2012.09.030.
[49] L. Wang, W.Q. Tao, L.Y. Yuan, Z.R. Liu, Q. Huang, Z.F. Chai, J.K. Gibson, W.Q. Shi, Rational control of the interlayer space inside two-dimensional titanium carbides for highly efficient uranium removal and imprisonment, Chem. Commun. 53 (89) (2017) 12084–12087, https://doi.org/10.1039/c7cc06740b.
[50] L. Wang, L.Y. Yuan, K. Chen, Y.J. Zhang, Q.H. Deng, S.Y. Du, Q. Huang, L.R. Zheng, J. Zhang, Z.F. Chai, M.W. Barsoum, X.K. Wang, W.Q. Shi, Loading Actinides in Multilayered Structures for Nuclear Waste Treatment: The First Case Study of Uranium Capture with Vanadium Carbide MXene, ACS Appl. Mater. Interfaces 8 (25) (2016) 16396–16403, https://doi.org/10.1021/acsami.6b02989.
[51] P.C. Zhang, L. Wang, K. Du, S.Y. Wang, Z.W. Huang, L.Y. Yuan, Z.J. Li, H.Q. Wang, L.R. Zheng, Z.F. Chai, W.Q. Shi, Effective removal of U(VI) and Eu(III) by carboxyl functionalized MXene nanosheets, J. Hazard. Mater. 396 (2020), 122731, https://doi.org/10.1016/j.jhazmat.2020.122731.
[52] Y.Z. Hu, C.F. Zhao, L. Yin, T. Wen, Y. Yang, Y.J. Ai, X.K. Wang, Combining batch technique with theoretical calculation studies to analyze the highly efficient enrichment of U(VI) and Eu(III) on magnetic $MnFe_2O_4$ nanocubes, Chem. Eng. J. 349 (2018) 347–357, https://doi.org/10.1016/j.cej.2018.05.070.
[53] M.L. Feng, D. Sarma, X.H. Qi, K.Z. Du, X.Y. Huang, M.G. Kanatzidis, Efficient Removal and Recovery of Uranium by a Layered Organic-Inorganic Hybrid Thiostannate, J. Am. Chem. Soc. 138 (38) (2016) 12578–12585, https://doi.org/10.1021/jacs.6b07351.
[54] S.L. Ma, L. Huang, L.J. Ma, Y. Shim, S.M. Islam, P.L. Wang, L.D. Zhao, S.C. Wang, G.B. Sun, X.J. Yang, M.G. Kanatzidis, Efficient Uranium Capture by Polysulfide/Layered Double Hydroxide Composites, J. Am. Chem. Soc. 137 (10) (2015) 3670–3677, https://doi.org/10.1021/jacs.5b00762.
[55] C.K. Jain, D.C. Singhal, M.K. Sharma, Adsorption of zinc on bed sediment of River Hindon: adsorption models and kinetics, J. Hazard. Mater. 114 (1–3) (2004) 231–239, https://doi.org/10.1016/j.jhazmat.2004.09.001.
[56] L. Wang, W.Q. Tao, E.Z. Ma, Z.J. Li, P. Ren, Y.J. Zhang, Z.R. Liu, L.Y. Yuan, W. Q. Shi, Thorium(IV) adsorption onto multilayered $Ti_3C_2T_x$ MXene: a batch, X-ray diffraction and EXAFS combined study, J. Synchrotron Radiat. 28 (2021) 1709–1719, https://doi.org/10.1107/S160057752101064x.
[57] S.X. Li, L. Wang, J. Peng, M.L. Zhai, W.Q. Shi, Efficient thorium(IV) removal by two-dimensional Ti_2CT_x MXene from aqueous solution, Chem. Eng. J. 366 (2019) 192–199, https://doi.org/10.1016/j.cej.2019.02.056.
[58] H.J. Chen, Y.Q. Wang, W.W. Zhao, G.X. Xiong, X.H. Cao, Y. Dai, Z.G. Le, Z. B. Zhang, Y.H. Liu, Phosphorylation of graphehe oxide to improve adsorption of U (VI) from aquaeous solutions, J. Radioanal. Nucl. Chem. 313 (1) (2017) 175–189, https://doi.org/10.1007/s10967-017-5274-2.
[59] X.J. Wang, G.J. Ji, G.R. Zhu, C.H. Song, H. Zhang, C.J. Gao, Surface hydroxylation of SBA-15 via alkaline for efficient amidoxime-functionalization and enhanced uranium adsorption, Sep. Purif. Technol. 209 (2019) 623–635, https://doi.org/10.1016/j.seppur.2018.07.039.
[60] Z.B. Zhang, X.F. Yu, X.H. Cao, R. Hua, M. Li, Y.H. Liu, Adsorption of U(VI) from aqueous solution by sulfonated ordered mesoporous carbon, J. Radioanal. Nucl. Chem. 301 (3) (2014) 821–830, https://doi.org/10.1007/s10967-014-3237-4.
[61] A.A. Galhoum, W.H. Eisa, I.E.T. El-Sayed, A.A. Tolba, Z.M. Shalaby, S. I. Mohamady, S.S. Muhammad, S.S. Hussien, T. Akashi, E. Guibal, A new route for manufacturing poly(aminophosphonic)-functionalized poly(glycidyl methacrylate)-magnetic nanocomposite - Application to uranium sorption from ore leachate, Environ. Pollut. 264 (2020), 114797, https://doi.org/10.1016/j.envpol.2020.114797.
[62] B.M. Jun, M. Jang, C.M. Park, J. Han, Y. Yoon, Selective adsorption of Cs^+ by MXene ($Ti_3C_2T_x$) from model low-level radioactive wastewater, Nucl. Eng. Technol. 52 (6) (2020) 1201–1207, https://doi.org/10.1016/j.net.2019.11.020.
[63] J. Jang, D.S. Lee, Magnetic Prussian Blue Nanocomposites for Effective Cesium Removal from Aqueous Solution, Ind. Eng. Chem. Res. 55 (13) (2016) 3852–3860, https://doi.org/10.1021/acs.iecr.6b00112.
[64] L. Wang, H. Song, L.Y. Yuan, Z.J. Li, Y.J. Zhang, J.K. Gibson, L.R. Zheng, Z.F. Chai, W.Q. Shi, Efficient U(VI) Reduction and Sequestration by Ti_2CT_x MXene, Environ. Sci. Tech. 52 (18) (2018) 10748–10756, https://doi.org/10.1021/acs.est.8b03711.
[65] Y.B. Sun, S.B. Yang, Y. Chen, C.C. Ding, W.C. Cheng, X.K. Wang, Adsorption and Desorption of U(VI) on Functionalized Graphene Oxides: A Combined Experimental and Theoretical Study, Environ. Sci. Tech. 49 (7) (2015) 4255–4262, https://doi.org/10.1021/es505590j.
[66] F.C. Wu, N. Pu, G. Ye, T.X. Sun, Z. Wang, Y. Song, W.Q. Wang, X.M. Huo, Y.X. Lu, J. Chen, Performance and Mechanism of Uranium Adsorption from Seawater to Poly(dopamine)-Inspired Sorbents, Environ. Sci. Tech. 51 (8) (2017) 4606–4614, https://doi.org/10.1021/acs.est.7b00470.

[67] X.P. Huang, X.J. Hou, F. Wang, B.H. Guo, F.H. Song, L. Ling, J.C. Zhao, L.Z. Zhang, Molecular-scale structures of uranyl surface complexes on hematite facets, Environ, Sci. Nano 6 (3) (2019) 892–903, https://doi.org/10.1039/c8en00899j.
[68] Y.M. Ren, H.L. Bao, Q. Wu, H.S. Wang, T. Gai, L. Shao, S.F. Wang, H. Tang, Y.R. Li, X.K. Wang, The physical chemistry of uranium (VI) immobilization on manganese oxides, J. Hazard. Mater. 391 (2020), 122207, https://doi.org/10.1016/j.jhazmat.2020.122207.
[69] H. O. Badr, V. Natu, S. Neațu, F. Neațu, A. Kuncser, A. Rostas, M.W. Barsoum, and M. Florea. Photo-stable, 1D-nanofilaments TiO_2-based lepidocrocite for photocatalytic hydrogen production in water-methanol mixtures, Matter 6 (2023), in press, https://doi.org/10.1016/j.matt.2023.05.026.
[70] O.R. Wilson, M.S. Carey, J.H. Cope, H.O. Badr, J.M. Nantz, T.A. ElMelegy, M. W. Barsoum, Repairable reinforced composites of 1D TiO_2 lepidocrocite mesoparticles and thiol-yne click networks via alkylborane-initiated in situ polymerization, Cell Rep. Phys. Sci. 4 (2023) 101434, https://doi.org/10.1016/j.xcrp.2023.101434.
[71] T. Sasaki, M. Watanabe, Y. Michiue, Y. Komatsu, F. Izumi, Preparation and Acid-Base Properties of a Protonated Titanate with the Lepidocrocitelike Layer, Chem. Mater. 7 (1995) 1001–1007, https://doi.org/10.1021/cm00053a029.
[72] T. Sasaki, M. Watanabe, H. Hashizume, H. Yamada, Macromolecule-like Aspects for a Colloidal Suspension of an Exfoliated Titanate. Pairwise Association of Nanosheets and Dynamic Reassembling Process Initiated from It, J. Am. Chem. Soc. 118 (1996) 8329–8335, https://doi.org/10.1021/ja960073b.